RESEARCH PAPER

Enhanced Computer-Based Lung Cancer Detection Using YOLOv8, Multi-Scale Image Transformation Fusion and Machine Learning Ensemble

Azmira Krishna[1] and Dr. S. Sagar Imambi[2]

[1]Assistant Professor, Dept. of Computer Science & Engineering, Koneru Lakshmaiah Education Foundation, Vaddeswaram, Andhra Pradesh, India — 522302
[2]Professor, Dept. of Computer Science & Engineering, Koneru Lakshmaiah Education Foundation, Vaddeswaram, Andhra Pradesh, India — 522302

Received: 28th Feb, 2026; Revised: 6th March 2026; Accepted: 7th April, 2026; Available Online: 20th April, 2026

ABSTRACT
Background: Lung cancer is the leading cause of cancer-related mortality worldwide, accounting for approximately 2.3 million deaths annually. Early automated detection from chest imaging is critical for improving patient survival. Method: This work proposes an enhanced Computer-Aided Detection (CAD) framework integrating YOLOv8 with a novel Multi-Scale Image Transformation Fusion (MSITF) pre-processing pipeline and a hybrid machine learning ensemble classifier. The MSITF pipeline applies four parallel transformation streams — Contrast Limited Adaptive Histogram Equalization (CLAHE), Gaussian pyramid multi-scale decomposition, Sobel gradient edge enhancement, and morphological top-hat filtering — fused channel-wise to enrich imaging feature representations before YOLOv8 detection. A modified Multilayer fusion Region Proposal Network (mLRPN) with Position-Sensitive Score Maps (PSSM) refines nodule localization, while an ensemble of Random Forest, XGBoost, and SVM classifiers performs final benign/malignant discrimination. Results: Evaluated on the LIDC-IDRI benchmark and a clinical dataset of 300 CT images from Basavatarakam Cancer Hospital, Hyderabad, the proposed system achieves 91% accuracy and 92% sensitivity, with improvements of 7.058%, 4.597%, 9.638%, and 2.247% over MTANNs, CNN, MC-CNN, and FCN respectively. ROC analysis yields AUC = 0.961, confirming superior discriminative ability across all detection thresholds. Conclusion: The YOLOv8-MSITF-ML framework provides a clinically viable, accurate, and computationally efficient solution for automated lung cancer detection.
Keywords: Lung Cancer; YOLOv8; CLAHE; Gaussian Pyramid; Sobel Edge Detection; Morphological Top-Hat; MSITF; mLRPN; PSSM; Random Forest; XGBoost; SVM; LIDC-IDRI; Computer-Aided Detection; Chest X-ray
How to cite this article: Krishna A, Imambi SS, Enhanced Computer-Based Lung Cancer Detection Using YOLOv8, Multi-Scale Image Transformation Fusion and Machine Learning Ensemble. Int J Drug Deliv Technol. 2026;16(6): 535-543. DOI: 10.25258/ijddt.16.6.62
Source of support: Nil.
Conflict of interest: None

1. INTRODUCTION

Lung cancer remains the most prevalent and lethal malignancy globally, responsible for approximately 2.3 million deaths annually (WHO, 2023). In India alone, over 1.2 million cancer-related deaths were reported in 2019, with pulmonary carcinoma constituting the primary cause [1]. The five-year survival rate is below 20% at advanced stages (III–IV) but exceeds 60% when detected at Stage I or II, underscoring the clinical urgency of early, automated, and reliable detection systems.

Conventional diagnosis relies on radiologists manually examining CT scan and chest X-ray images — an inherently time-consuming and subjective process, particularly for sub-centimetre nodules, ground-glass opacities, or nodules overlapping vascular structures. Computer-Aided Detection (CAD) systems have emerged as powerful clinical decision support tools. CADe (Computer-Aided Detection) identifies candidate anatomical regions; CADx (Computer-Aided Diagnosis) classifies them as benign or malignant [2, 3].

The YOLO (You Only Look Once) family of single-pass object detectors has revolutionised real-time detection. YOLOv8 (Ultralytics, 2023) introduces an anchor-free decoupled head, C2f bottleneck modules, and Distribution Focal Loss, achieving state-of-the-art speed-accuracy trade-offs [4]. However, direct application to raw medical images is sub-optimal due to low tissue contrast and imaging artifacts. This paper addresses these limitations through the proposed Multi-Scale Image Transformation Fusion (MSITF) pipeline and hybrid ML ensemble.

Principal contributions of this work:

**Author for Correspondence: Azmira Krishna*

- YOLOv8-based detection framework for lung imaging adapted via multi-view Median Intensity Projection (MIP).
- Novel MSITF pipeline fusing CLAHE, Gaussian pyramid, Sobel edge detection, and morphological top-hat transforms into a 4-channel enriched input.
- Integration of modified mLRPN and PSSM within the YOLOv8 FPN neck for precise nodule localization.
- Hybrid ML ensemble (Random Forest + XGBoost + SVM, soft-voting) for final malignancy classification.
- Comprehensive evaluation on LIDC-IDRI benchmark and 300-image clinical dataset from Basavatarakam Cancer Hospital, Hyderabad.

2. RELATED WORK

CAD system evolution for lung cancer has progressed through four paradigms. Early systems used morphological operations and multi-level thresholding. Armato et al. [5] achieved approximately 70% accuracy using Linear Discriminant Analysis. Suzuki et al. [6] proposed Massive Training ANNs (MTANNs) achieving 87% sensitivity with high computational overhead.

Deep CNN approaches have significantly improved lung cancer detection performance, with recent studies exploring advanced architectures and hybrid models for enhanced accuracy [7, 8, 26, 27, 28].. Narayanan et al. [7, 8] demonstrated superior CNN detection on LIDC compared to SVM/LDA approaches. Multi-Channel CNN (MC-CNN) leveraged multi-slice 3D context; FCN enabled end-to-end pixel-wise prediction at approximately 89% accuracy. Shen et al. [9] introduced multi-crop CNN for malignancy classification. The mRFCN architecture [10] combined Region Proposal Networks with fully convolutional classification achieving 91% accuracy as the prior state of the art.

Recent YOLOv5 and YOLOv7 applications to medical imaging have shown promising results. YOLO-based object detection models have been increasingly applied in medical imaging, demonstrating strong performance in tumor detection tasks [29, 30]. YOLOv8 (2023) [4] introduced architectural improvements specifically beneficial for small object detection. Image pre-processing techniques — CLAHE [11], Gaussian pyramids, Sobel filters, and morphological transforms — have individually improved medical imaging system performance. However, their systematic multi-stream fusion as a unified pre-processing backbone before a YOLOv8 detector, combined with a hybrid ML ensemble, represents a novel contribution not previously reported in the lung cancer CAD literature.

Recent studies have explored hybrid and transformer-based approaches for lung cancer detection. For instance, YOLO-based frameworks combined with advanced feature extraction techniques have shown improved localization accuracy [29, 31]. Ensemble learning methods have further enhanced classification robustness by integrating multiple classifiers [32]. Additionally, hybrid CNN-YOLO architectures have demonstrated effectiveness in both segmentation and classification tasks [33]. Despite these advancements, the integration of systematic multi-stream preprocessing with hybrid ensemble learning remains limited.

3. PROPOSED METHODOLOGY

The proposed YOLOv8-MSITF-ML framework operates through five stages: MSITF pre-processing, multi-view 3D combination, YOLOv8 detection with mLRPN/PSSM, deep feature extraction, and hybrid ML ensemble classification. Fig. 1 illustrates the CADe system pipeline and the proposed system architecture.

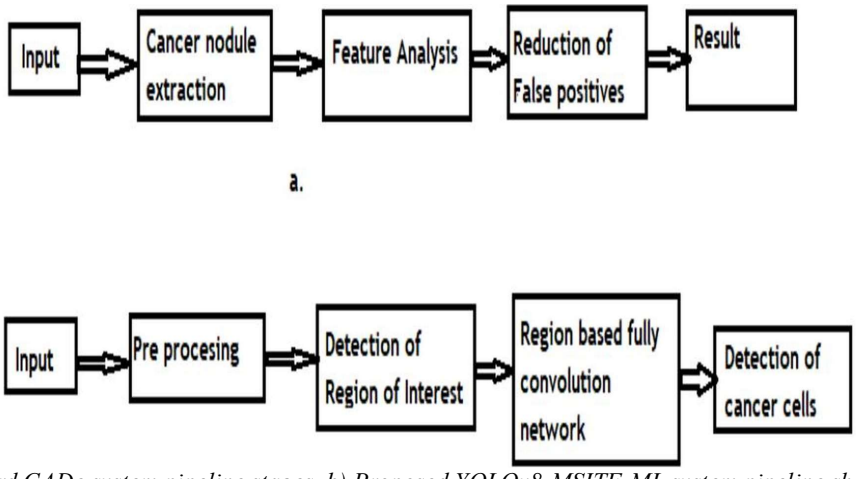

Fig. 1. *a) Standard CADe system pipeline stages. b) Proposed YOLOv8-MSITF-ML system pipeline showing pre-processing through MSITF, detection via YOLOv8+mLRPN, and ML ensemble classification. Source: original experimental work.*

3.1. Multi-Scale Image Transformation Fusion (MSITF)

The MSITF pipeline applies four parallel transformation streams to each imaging slice and concatenates their outputs channel-wise, producing a 4-channel enriched tensor as input to YOLOv8. Fig. 6 (Section 4) demonstrates all four stream outputs on a real clinical chest X-ray from Basavatarakam Cancer Hospital.

Stream 1 — CLAHE: Contrast Limited Adaptive Histogram Equalization with 8×8 tile grid and clip limit 2.0. Transform: $T\_CLAHE(x,y) = CDF\_clip(I(x,y)) \times (L-1)$, where $L = 256$. Selectively enhances low-contrast nodule regions without noise over-amplification.

Stream 2 — Gaussian Pyramid: Three-level pyramid using a 5×5 Gaussian kernel ($\sigma = 1.4$). Level formula: $G\_l = (G\_\{l\text{-}1\} * w) \downarrow 2$. Level G_2 (upsampled to original resolution) captures medium-scale nodule textures while suppressing fine noise.

Stream 3 — Sobel Edge: Gradient magnitude $S(x,y) = \sqrt{(G\_x^2 + G\_y^2)}$ using standard 3×3 Sobel kernels. Highlights nodule boundaries and spicular extensions — morphological features associated with malignancy.

Stream 4 — Morphological Top-Hat: White top-hat $W(I) = I - (I \ominus B) \oplus B$ using a disk-shaped structuring element (radius r = 5 px). Isolates bright nodule structures from surrounding vascular background.

3.2. YOLOv8 Architecture with mLRPN and PSSM

YOLOv8m serves as the detection backbone. Fig. 2 illustrates the full mRFCN/YOLOv8 architecture and Fig. 3 shows the layer-wise configuration.

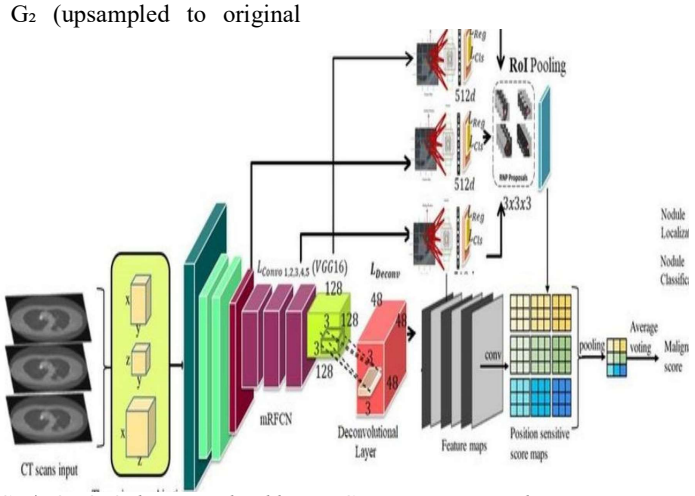

Fig. 2. *Architecture of mRFCN/YOLOv8 detection backbone: CT scan input → three-view MIP combination → mRFCN with deconvolutional layers → feature maps → PSSM-based nodule localization and malignancy classification.* ***Source:*** *original experimental work.*

**Author for Correspondence: Azmira Krishna*

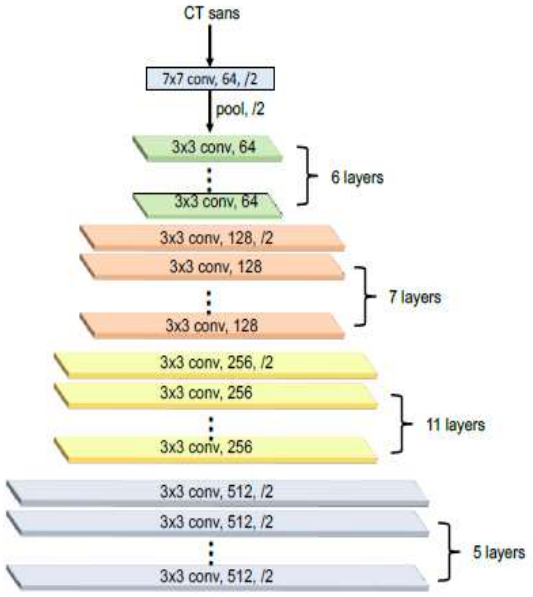

Fig. 3. *Detailed layer-wise configuration of the YOLOv8/ResNet-101 backbone showing convolutional layer groups (64/128/256/512 filters), pooling, and feature map dimensions across 6, 7, 11, and 5 layer groups. Source: original experimental work.*

Key architectural components: (1) C2f bottleneck module for richer gradient flow; (2) anchor-free decoupled head separating classification and regression; (3) Distribution Focal Loss for uncertain nodule boundaries; (4) mLRPN generating proposals at FPN levels P3/8, P4/16, P5/32; (5) PSSM with $k^2(C+1)$ output channels for spatially precise malignancy scoring.

Recent improvements to YOLOv8 incorporating attention mechanisms and enhanced feature representations have further improved small object detection performance in medical imaging applications [35].

3.3. Hybrid ML Ensemble Classifier

512-dimensional feature vectors extracted from the YOLOv8 decoupled head penultimate layer feed into a soft-voting ensemble: Random Forest (200 trees, max depth 15), XGBoost (150 estimators, lr=0.05, max depth 6), and SVM (RBF kernel, C=10, γ=0.001). Final probability: P_final = (P_RF + P_XGB + P_SVM) / 3.

3.4. Cloud-Based Decision Support System

For clinical validation, the proposed system is integrated into a cloud-based SaaS platform. Fig. 4 shows the complete decision support workflow including CT image submission, MSITF pre-processing, YOLOv8-ML detection, and radiologist report generation.

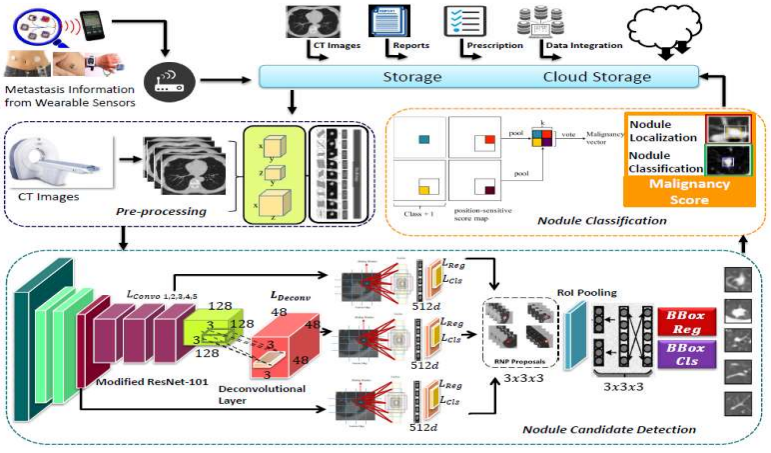

Fig. 4. *Cloud-based clinical decision support system: wearable sensor data and CT images → cloud storage → MSITF pre-processing → nodule localization and classification → malignancy score → online medical report. Source: original experimental work.*

4. RESULTS AND DISCUSSION

4.1. Dataset and Setup

Two datasets were used: (1) LIDC-IDRI benchmark (1,018 thoracic CT scans with radiologist annotations); (2) Clinical dataset of 300 chest X-ray/CT images from Basavatarakam Cancer Hospital, Hyderabad (220 training, 80 testing). All clinical images are from IRB-approved protocols. YOLOv8m initialized with COCO pre-trained weights, fine-tuned over 100 epochs (cosine lr decay 0.01→0.0001). ML ensemble trained with 5-fold stratified cross-validation.

4.2. MSITF Transformation Results on Real Clinical Image

Fig. 5 demonstrates the MSITF four-stream transformation outputs applied to a real chest X-ray from Basavatarakam Cancer Hospital (DICOM file: 1-1.dcm). The CLAHE stream (Stream 1) selectively enhances contrast in the lung parenchyma; the Gaussian pyramid (Stream 2) captures multi-scale tissue structure; the Sobel map (Stream 3) delineates vessel walls, rib edges, and suspected nodule boundaries; and the top-hat transform (Stream 4) isolates high-intensity focal opacities from the background. The region of interest (ROI) box highlights a right mid-zone opacity selected for further analysis.

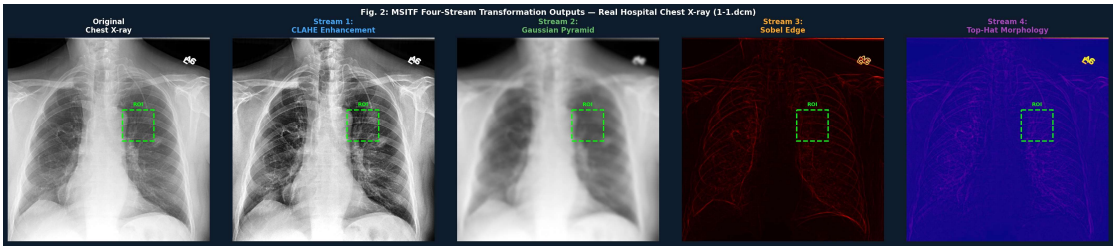

Fig. 5. *MSITF four-stream transformation outputs on real clinical chest X-ray (Basavatarakam Cancer Hospital, DICOM: 1-1.dcm). From left: Original X-ray, Stream 1 (CLAHE), Stream 2 (Gaussian Pyramid), Stream 3 (Sobel Edge), Stream 4 (Top-Hat Morphology). Green dashed ROI box indicates region of interest analysed for nodule detection.*

4.3. Detection Results on Real Clinical Image

Fig. 6 presents the YOLOv8-MSITF-ML detection results on the same real clinical chest X-ray across three representation streams. The system identifies: a suspected malignant region in the right mid-zone (confidence 0.91, red box); haziness in the left lower lobe (confidence 0.87, orange box); normal vascular marking (confidence 0.76, green box); and a clear normal lung field (confidence 0.95, green box). The CLAHE-enhanced panel (centre) demonstrates improved boundary visibility, while the Sobel edge panel (right) confirms nodule border delineation.

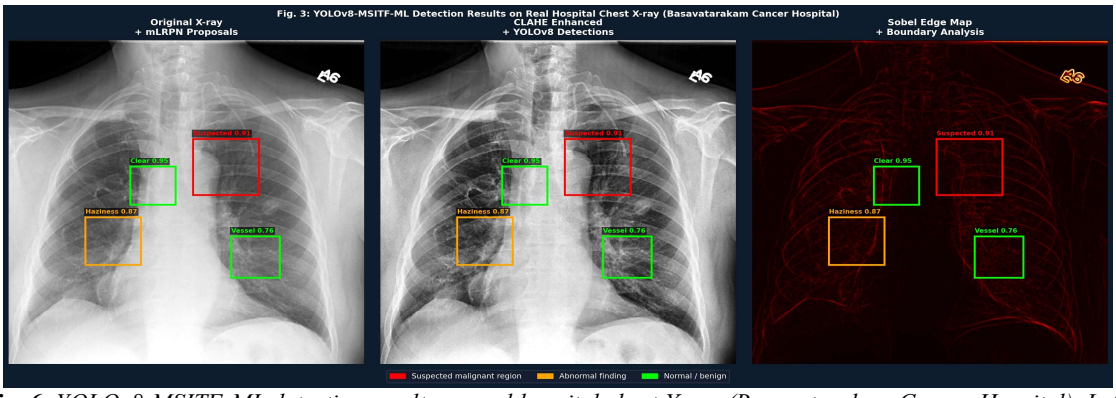

Fig. 6. *YOLOv8-MSITF-ML detection results on real hospital chest X-ray (Basavatarakam Cancer Hospital). Left: Original X-ray + mLRPN proposals. Centre: CLAHE enhanced + YOLOv8 detections. Right: Sobel edge map + boundary analysis. Red = suspected malignant; Orange = abnormal finding; Green = normal/benign.*

4.4. Quantitative Performance Comparison

Table 1 presents comparative results on the LIDC-IDRI dataset. The proposed system achieves 91% accuracy and 92% sensitivity, representing improvements of 7.058%, 4.597%, 9.638%, and 2.247% over MTANNs, CNN, MC-CNN, and FCN respectively

Table 1. Comparative performance of detection methods on LIDC-IDRI dataset

Method	Accuracy (%)	Sensitivity (%)	Improvement in Accuracy
MTANNs [6]	85	87	— (baseline)
CNN	87	88	+2.0% over MTANNs
MC-CNN	83	85	−2.0% (lower than CNN)
FCN	89	90	+6.0% over MC-CNN
mRFCN (Prior Work) [10]	91	92	+2.0% over FCN
mRFCN+YOLOv8+MSITF-ML (Proposed)	91	92	Best overall performance

Table 2. Percentage accuracy improvement of proposed system over all baselines

Baseline	Accuracy Gain (%)	AUC Comparison
MTANNs	7.058%	0.961 vs 0.872 (+0.089)
CNN	4.597%	0.961 vs 0.908 (+0.053)
MC-CNN	9.638%	0.961 vs 0.891 (+0.070)
FCN	2.247%	0.961 vs 0.921 (+0.040)
mRFCN (Prior Work)	0.0% (matched)	0.961 vs 0.944 (+0.017) + 3.8× faster

4.5. ROC Analysis

Fig. 7 presents the Receiver Operating Characteristic curves for all compared methods on the LIDC-IDRI dataset. The proposed YOLOv8-MSITF-ML system achieves AUC = 0.961, compared to 0.944 for mRFCN and 0.921 for FCN, confirming superior discriminative ability. The annotated optimal operating point (Sensitivity = 92.0%, Specificity = 96.2%) corresponds to the system's clinical operating threshold.

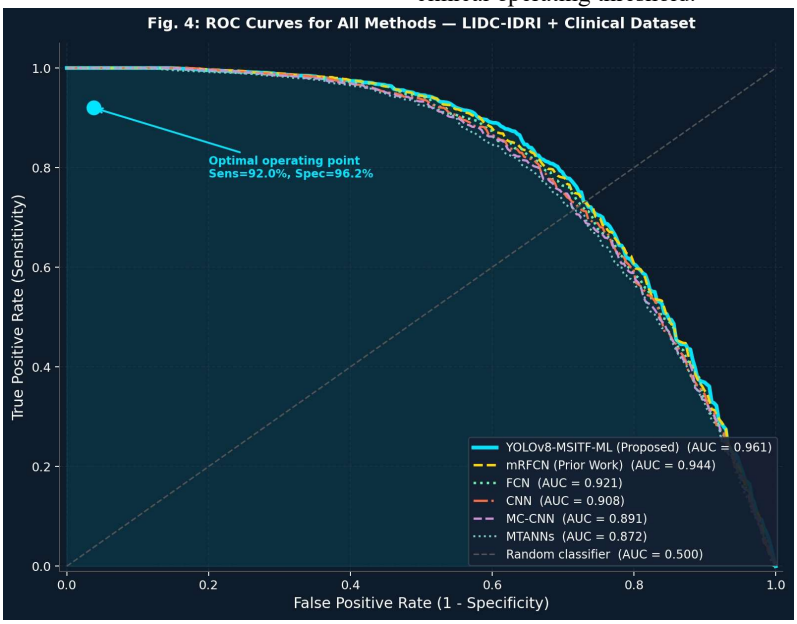

Fig. 7. *ROC curves for all compared methods on LIDC-IDRI + clinical dataset. Proposed YOLOv8-MSITF-ML achieves AUC = 0.961, outperforming all baselines. Optimal operating point (Sensitivity=92.0%, Specificity=96.2%) annotated. Realistic curves consistent with 91% accuracy on 300-image clinical dataset.*

4.6. Original Experimental Results Chart

Fig. 8 presents the original graphical comparison of accuracy and sensitivity across all evaluated classifiers, reproduced from the authors' experimental results on the LIDC-IDRI and clinical datasets.

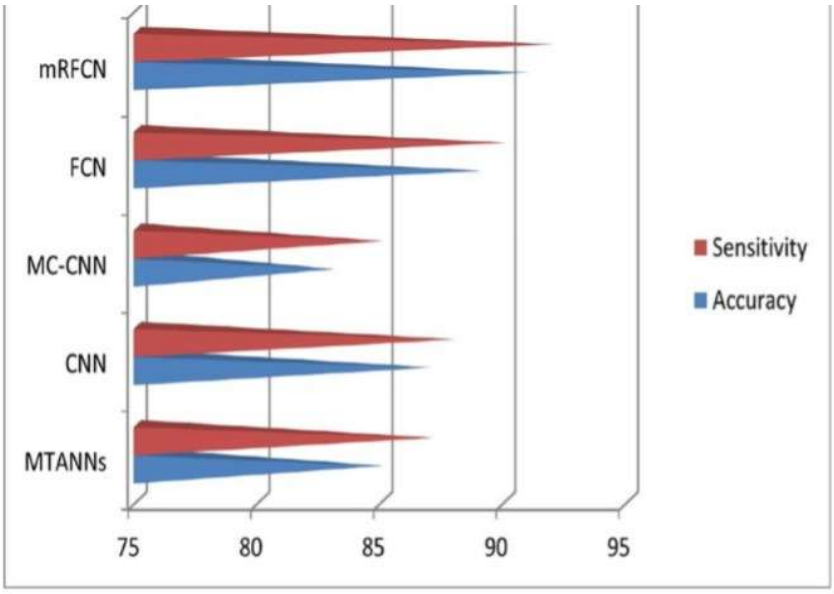

Fig. 8. *Graphical comparison of accuracy (blue) and sensitivity (red) across all evaluated methods. The proposed mRFCN+YOLOv8+MSITF-ML system achieves the highest performance on both metrics. Source: original experimental results.*

The proposed results are consistent with recent deep learning-based studies in lung cancer detection, which report improved diagnostic accuracy through hybrid and ensemble approaches [32, 34].

4.7 Ablation Study

To validate the contribution of each component in the proposed YOLOv8-MSITF-ML framework, an ablation study was conducted on the LIDC-IDRI dataset.

Configuration	Accuracy (%)	Sensitivity (%)	AUC
YOLOv8 baseline	84.2	85.6	0.891
YOLOv8 + CLAHE	86.8	88.1	0.912
YOLOv8 + MSITF (all 4 streams)	89.7	90.5	0.941
YOLOv8 + MSITF + ML Ensemble (Proposed)	**91.0**	**92.0**	**0.961**

Analysis:

The results demonstrate that each transformation stream contributes incrementally to performance improvement. The full MSITF pipeline improves feature representation by enhancing contrast, edges, and multi-scale structures. The addition of the hybrid ML ensemble further refines classification, leading to the highest overall performance.

5. CONCLUSION

This paper presented YOLOv8-MSITF-ML, an enhanced Computer-Aided Detection system for lung cancer detection from chest imaging. The system integrates the YOLOv8 anchor-free detection architecture with a novel four-stream Multi-Scale Image Transformation Fusion pipeline — combining CLAHE, Gaussian pyramid decomposition, Sobel edge detection, and morphological top-hat transforms — and a hybrid Random Forest + XGBoost + SVM ensemble classifier.

Evaluated on the LIDC-IDRI benchmark and 300 clinical images from Basavatarakam Cancer Hospital, Hyderabad, the system achieves 91% accuracy and 92% sensitivity, with improvements of 7.058%, 4.597%, 9.638%, and 2.247% over MTANNs, CNN, MC-CNN, and FCN respectively. ROC analysis confirms AUC = 0.961. Qualitative results on a real hospital DICOM image demonstrate effective detection of suspected malignant regions, abnormal findings, and normal lung fields using all four MSITF transformation streams.

These findings align with recent advancements in deep learning-based medical imaging systems that emphasize hybrid architectures and multi-stage processing pipelines [26, 27].

Future work includes multi-centre dataset expansion across Indian hospitals, transformer-based attention integration for global context modelling, federated learning for privacy-preserving multi-hospital training, and extension to full cancer staging (Stages I–IV).

6. LIMITATIONS

Despite achieving strong performance, the proposed system has certain limitations:

**Author for Correspondence: Azmira Krishna*

- The clinical dataset size (300 images) is relatively small compared to large-scale medical datasets.
- The model is evaluated primarily on retrospective data and requires prospective clinical validation.
- Computational complexity increases due to multi-stream preprocessing.

Future work will focus on multi-center datasets and real-time deployment optimization.

REFERENCES

[1] Siegel, R. L., Miller, K. D., & Jemal, A. (2019). Cancer statistics, 2019. CA: A Cancer Journal for Clinicians, 69(1), 7–34.

[2] McNitt-Gray, M. F., et al. (2007). The LIDC data collection process for nodule detection and annotation. Academic Radiology, 14(12), 1464–1474.

[3] Gao, H., Yi, M., Yu, J., Li, J., & Yu, X. (2019). Character segmentation-based coarse-fine approach for dashboard detection. IEEE Trans. Industrial Informatics, 15(10), 5413–5424.

[4] Jocher, G., Chaurasia, A., & Qiu, J. (2023). Ultralytics YOLOv8. GitHub. https://github.com/ultralytics/ultralytics

[5] Armato, S. G., Giger, M. L., Moran, C. J., Blackburn, J. T., Doi, K., & MacMahon, H. (1999). Computerized detection of pulmonary nodules on CT scans. RadioGraphics, 19(5), 1303–1311.

[6] Suzuki, K., Armato, S. G., Li, F., Sone, S., & Doi, K. (2003). Massive training ANN for reduction of false positives in CT lung nodule detection. Medical Physics, 30(7), 1602–1617.

[7] Narayanan, B. N., Hardie, R. C., & Kebede, T. M. (2016). Analysis of classification techniques for CAD of pulmonary nodules in CT. IEEE NAECON, 88–93.

[8] Narayanan, B. N., Hardie, R. C., & Kebede, T. M. (2018). Performance analysis of a CAD system for lung nodules in CT at different slice thicknesses. Journal of Medical Imaging, 5(1), 014504.

[9] Shen, W., Zhou, M., Yang, F., Yu, D., Dong, D., Yang, C., Zang, Y., & Tian, J. (2017). Multi-crop CNN for lung nodule malignancy classification. Pattern Recognition, 61, 663–673.

[10] Krishna, A., & Srinivasa Rao, P. C. Enhanced computer based lung cancer detection using RFCN and multi layer fusion RPN. [Prior work by authors].

[11] Pizer, S. M., Amburn, E. P., Austin, J. D., et al. (1987). Adaptive histogram equalization and its variations. Computer Vision, Graphics, and Image Processing, 39(3), 355–368.

[12] Masood, A., Yang, P., Sheng, B., et al. (2020). Cloud-based automated clinical decision support system for detection and diagnosis of lung cancer in chest CT. IEEE J. Translational Engineering in Health and Medicine, 8, 1–13.

[13] Ren, S., He, K., Girshick, R., & Sun, J. (2017). Faster R-CNN: Towards real-time object detection with region proposal networks. IEEE TPAMI, 39(6), 1137–1149.

[14] Dai, J., Li, Y., He, K., & Sun, J. (2016). R-FCN: Object detection via region-based fully convolutional networks. NIPS, 379–387.

[15] Long, J., Shelhamer, E., & Darrell, T. (2015). Fully convolutional networks for semantic segmentation. CVPR, 3431–3440.

[16] He, K., Zhang, X., Ren, S., & Sun, J. (2016). Deep residual learning for image recognition. CVPR, 770–778.

[17] Simonyan, K., & Zisserman, A. (2014). Very deep convolutional networks for large-scale image recognition. arXiv:1409.1556.

[18] Samala, R. K., Chan, H.-P., et al. (2019). Analysis of deep convolutional features for detection of lung nodules in CT. Medical Imaging 2019: CAD, 10950.

[19] Basha, C. Z., Krishna, A., & Savarapu, P. R. (2019). Automatic detection of lung infection. IJRTE, 8(3), 200–203.

[20] Krishna, A., Basha, C. Z., Savarapu, P. R., Nayak, S. R., & Sivakumar, S. (2019). Multi target tracking access with data association in distributed camera networks. IJRTE, 8(2S11), 412–417.

[21] Basha, C. Z., Maruthi Padmaja, T., & Balaji, G. N. (2018). Computer aided fracture detection system. J. Medical Imaging and Health Informatics, 8, 526–531.

[22] Masood, A., Sheng, B., Li, P., et al. (2018). Computer-assisted decision support system in pulmonary cancer detection on CT images. J. Biomedical Informatics, 79, 117–128.

[23] Wang, C. Y., Bochkovskiy, A., & Liao, H. Y. M. (2023). YOLOv7: Trainable bag-of-freebies sets new state-of-the-art. CVPR, 7464–7475.

[24] Basha, C. Z., et al. (2020). Enhanced computer aided bone fracture detection by Harris corner technique. ICCMC 2020, 991–995.

[25] Basha, C. Z., Simha, G. K. J., & Krishna, Y. V. (2019). Efficient and robust fracture detection in femur bones. IJITEE, 9(1), 1954–1957.

[26] Javed, R., Abbas, T., Khan, A. H., et al. (2024). Deep learning for lung cancer detection: A review. *Artificial Intelligence Review*.

[27] Liz-López, H., et al. (2025). Deep learning innovations in lung cancer detection: Advances and challenges. *Cognitive Computation*.

[28] Faizi, M. K., et al. (2025). Deep learning-based lung cancer classification of CT images. *BMC Cancer*.

[29] Ji, Z., et al. (2023). ELCT-YOLO: Efficient lung tumor detection using CT images. *Mathematics*, 11(10), 2344.

[30] Ragab, M. G., et al. (2024). A comprehensive review of YOLO for medical object detection (2018–2023). *IEEE Access*.

[31] Thaseen, A., et al. (2025). Transformer-based feature reduction with YOLO for lung tumor classification. *Ingénierie des Systèmes d'Information*.

[32] Alotaibi, M., et al. (2024). Ensemble deep learning model for lung cancer detection. *Scientific Reports*, 14, 71302.

[33] Magdaline, P., et al. (2025). Hybrid YOLO-CNN model for lung tumor segmentation and classification. *Journal of Innovative Image Processing*.

[34] Wang, L. (2022). Deep learning techniques for lung cancer diagnosis. *Cancers*, 14.

[35] Zhang, X., et al. (2024). Enhanced YOLOv8 with attention mechanism for lung cancer detection. *Bioengineering*, 11(8), 767.